A method of constructing phyllotaxically arranged modular models by partitioning the interior of a cylinder or a cone

Cezary Stępień
Institute of Computer Science, Warsaw University of Technology, Poland
cst@ii.pw.edu.pl

Abstract. The paper describes a method of partitioning a cylinder space into three-dimensional subspaces, congruent to each other, as well as partitioning a cone space into subspaces similar to each other. The way of partitioning is of such a nature that the intersection of any two subspaces is the empty set. Subspaces are arranged with regard to phyllotaxis. Phyllotaxis lets us distinguish privileged directions and observe parastichies trending these directions. The subspaces are created by sweeping a changing cross-section along a given path, which enables us to obtain not only simple shapes but also complicated ones. Having created these subspaces, we can put modules inside them, which do not need to be obligatorily congruent or similar. The method ensures that any module does not intersect another one. An example of plant model is given, consisting of modules phyllotaxically arranged inside a cylinder or a cone.

Key words: computer graphics; modeling; modular model; phyllotaxis; cylinder partitioning; cone partitioning; genetic helix; parastichy.

1. Introduction

Phyllotaxis is the manner of how leaves are arranged on a plant stem. The regularity of leaves arrangement, known for a long time, still absorbs the attention of researchers in the fields of botany, mathematics and computer graphics. Various methods have been used to describe phyllotaxis. A historical review of problems referring to phyllotaxis is given in [7]. Its connections with number sequences, e.g. Fibonacci sequence, and with problems of symmetry, the golden ratio and logarithmic spiral have been discussed in a number of papers. A few theories of biological processes and biomechanical phenomena resulting in appropriate phyllotactic patterns were put forward ([9] - [14]). Douady and Couder [2], [5] showed that phyllotactic patterns similar to those observed in botany can also emerge as a result of activity of other physical processes. This approach is continued in [16], where a magnetic cactus is presented. The influence of basic parameters on a kind of phyllotactic pattern of both theoretical models and real plants is described in [4], [15]. The paper [8] contains a uniform description of spiral, jugate and whorl patterns on the basis of Helmholtz equation. Papers [1], [3] present an application of phyllotactic patterns to plant modeling in computer graphics. The website [17] shows that phyllotaxis

can be an inspiration for architects. The aim of this paper is to propose a new method of constructing objects being a set of modules arranged inside a cylinder or a cone in such a manner that they satisfy the rules of phyllotaxis. The modules are analogs of leaves and for this reason they cannot intersect. In order to obtain the appropriate result, a conception of subspaces is introduced. The subspaces fill to capacity the space of a model. Each subspace can contain exactly one module. The subspaces are obliged to satisfy appropriate conditions in reference to other subspaces while modules being analogs of leaves should be in appropriate relations, each to its own subspace.

In Chapter 2, fundamental conceptions referring to phyllotaxis are introduced, such as genetic helix or parastichy. In Chapter 3, the flat model of two- and three-directional phyllotaxis is introduced. Chapter 4 describes phyllotaxis on cylindrical and conical surfaces. Chapter 5 describes partitioning the interior of a cylinder and a cone. In Chapter 6, a method of arranging modules using subspaces is presented and Chapter 7 contains a conclusion.

2. Genetic helix and parastichies

To describe phyllotaxis, an arrangement of modules on a cylindrical surface of the radius R is often studied. The cylinder axis lies on the z axis of the coordinate system. As a result of the growing process, the module $i+1$ emerges on the surface of the cylinder in such a manner that it is rotated by a fixed angle $\Delta\alpha$ and moved by a fixed distance Δz along z axis, both in reference to the module i.

Let $i = 0, \pm1, \pm2,...$ Knowing the origin coordinates of the module i, i.e. its angle α_i and its axis position z_i we can calculate the position of the next point from the equations: $\alpha_{i+1} = \alpha_i + \Delta\alpha$, $z_{i+1} = z_i + \Delta z$, so that we obtain a sequence of points $Q = \{\mathbf{q}_i\}$ lying on a helix. We call this helix a *genetic helix* and $\Delta\alpha$—an *angle of divergence* [7].

Let a natural number N be given. Having the sequence Q, create a subsequence Q_j^N, $(j = 0, 1,... N-1)$, choosing elements $\mathbf{q}_j$, $\mathbf{q}_{j\pm N}$, $\mathbf{q}_{j\pm 2N}$,... Connect these points using a line being a helix. We call this helix *parastichy of the order* N and mark them with a symbol P_j^N.

If two numbers N_1 and N_2 $(N_1 \neq N_2)$ are given instead of the number N, then we can study two sets of parastichies $\{P_j^{N_1}\}$ and $\{P_k^{N_2}\}$, where $j = 0, 1,... N_1 - 1$ and $k = 0, 1,... N_2 - 1$. Parastichies belonging to the same set do not intersect in opposition to parastichies belonging to different sets, as the latter ones intersect in certain points of Q.

Figure 1(a) represents a genetic helix, Fig. 1(b) and 1(c) show two examples of sets $\{P_j^{N_1}\}$ and $\{P_j^{N_2}\}$ and Fig. 1(d) shows an example of three sets of parastichies.

One can cut open the cylindrical surface and study the genetic helix in a two-dimensional space $S^{<\alpha\zeta>}$, i.e. in a space with the coordinate system $O\alpha\zeta$, where $\alpha \in \langle -\pi, \pi)$ and $\zeta \in (-\infty, +\infty)$. In this case α is the angle and ζ stands for z. On

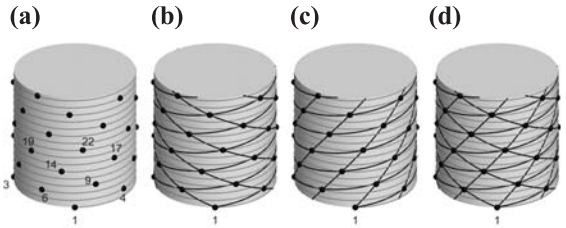

Fig. 1. Genetic helix (a) and parastichies belonging to sets: (b) $\{P_j^3\}$, $\{P_k^5\}$, (c) $\{P_j^3\}$, $\{P_k^8\}$, and (d) $\{P_j^3\}$, $\{P_k^5\}$, $\{P_l^8\}$.

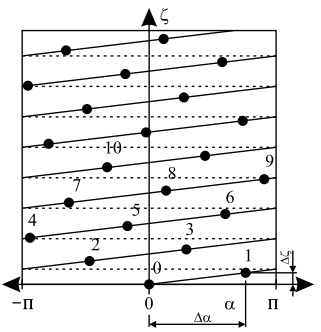

Fig. 2. The genetic helix on the cut open and unrolled cylinder surface.

a conical surface, the dependence of z upon ζ is slightly more complicated, which is described in Chapter 4.

In the case of two-dimensional space $S^{<\alpha\zeta>}$, the genetic helix and parastichies change into sets of line sections moved along the z axis by a constant value [1].

3. Flat model of phyllotaxis

In order to define a genetic helix in the space $S^{<\alpha\zeta>}$, we need two parameters $\Delta\alpha$ and $\Delta\zeta$. We calculate coordinates of points $\mathbf{q}_i$ using equations:

$$\alpha_i = \Delta\alpha\, i - 2\pi k,$$
$$\zeta_i = \Delta\zeta\, i,$$

where k: $\alpha_i \in \langle -\pi, \pi)$ and $i = 0, \pm1, \pm2,...$

The genetic helix for $\zeta \geq 0$ is shown in Figure 2. Notice that the genetic helix passes through the point $\mathbf{q}_0$ of coordinates $(\alpha, \zeta) = (0, 0)$.

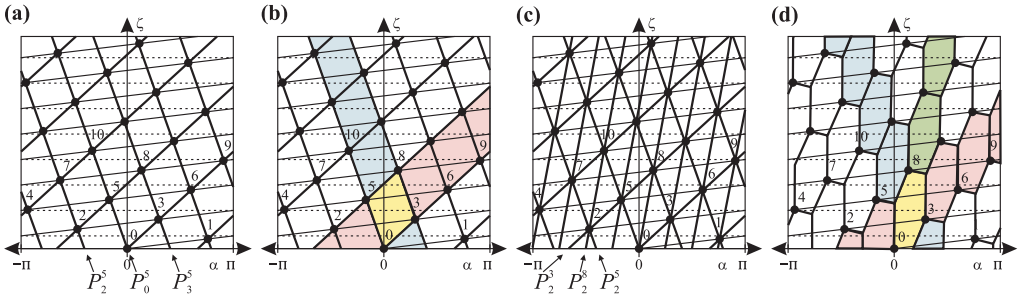

Fig. 3. The space with parastichies belonging to sets: (a) $\{P_j^3\}$, $\{P_k^5\}$ and (c) $\{P_j^3\}$, $\{P_k^5\}$, $\{P_l^8\}$ and partitioning the space into parallelograms and hexagons.

Figure 3(a) shows parastichies belonging to sets $\{P_j^{N_1}\}$ and $\{P_k^{N_2}\}$ where $N_1 = 3$ and $N_2 = 5$. For each parastichy of the order $N \geq 3$, it is possible to show two parastichies belonging to the same set and being in neighborhood with it. In this figure, we see that the parastichy P_0^5 is a neighbor of P_2^5 and P_3^5. In accordance with two directions constituted by two sets of parastichies one can divide the space $S^{<\alpha\zeta>}$ into parallelograms of identical shapes and orientations filling all the space (Figure 3(b)). The parallelograms, due to their contact by their sides, create strips in accordance with the parastichies directions. We call such partitioning a *two-directional* one.

Analogically, we can consider three sets of parastichies $\{P_j^{N_1}\}$, $\{P_k^{N_2}\}$ and $\{P_l^{N_1+N_2}\}$. Such case was studied in [1]. The set $\{P_l^{N_1+N_2}\}$ states the third direction, as it is shown in Figure 3(c) for the sets $\{P_j^3\}$, $\{P_k^5\}$ and $\{P_l^8\}$. Then we can divide the space into hexagons of identical shapes and orientations completely filling it out. In Figure 3(d) we can observe strips parallel to these three directions and so we call such partitioning a *three-directional* one.

Instead of $\{P_l^{N_1+N_2}\}$ we can take into account the set $\{P_l^{N_1-N_2}\}$ $(N_1 - N_2 \geq 1)$ [1], but that case can be easily reduced to the case described above.

Below, we study two- and three directional partitionings into areas of identical shapes and orientations, but we do not demand their sides to be sections of straight lines.

Firstly, we will consider a three directional partitioning. Let there be given the point $\mathbf{q}_i$ lying in the place, where parastichies $P_j^{N_1}$, $P_k^{N_2}$ and $P_l^{N_1+N_2}$ intersect. We also consider points lying on neighboring parastichies, namely $\mathbf{q}_{i+N_1}$, $\mathbf{q}_{i+N_2}$, and $\mathbf{q}_{i+N_1+N_2}$.

Assume that the point $\mathbf{q}_i$ is associated with two points $\mathbf{v}_i^{<1>}$, $\mathbf{v}_i^{<2>}$ and with a line L_i consisting of three open line segments $L_i^{<1>}$, $L_i^{<2>}$ and $L_i^{<3>}$, as it is shown in Figure 4(a). These line segments can be fragments of straight lines, curves or polylines. We assume below that for each two points $\mathbf{q}_{i_1}$ and $\mathbf{q}_{i_2}$ these lines are congruent in couples:

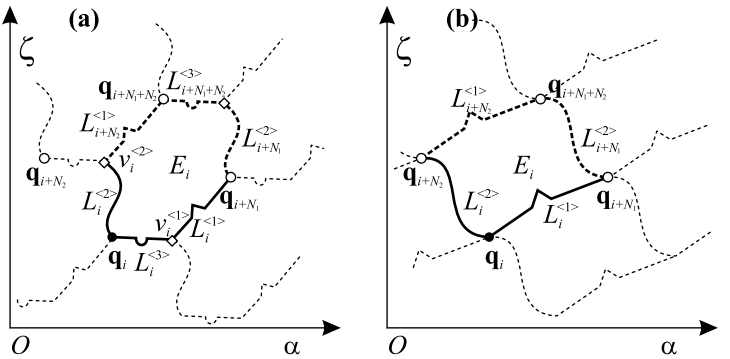

Fig. 4. Example of (a) three-directional partitioning and (b) two directional one.

$$L_{i_1}^{<1>} \equiv L_{i_2}^{<1>}, \quad L_{i_1}^{<2>} \equiv L_{i_2}^{<2>}, \quad L_{i_1}^{<3>} \equiv L_{i_2}^{<3>}. \tag{1}$$

From this assumption it appears that $\mathbf{v}_i^{<1>} = \mathbf{v}_{i-N_2}^{<2>}$ and $\mathbf{v}_i^{<2>} = \mathbf{v}_{i+N_2}^{<1>}$.

The segments $L_i^{<1>}$, $L_i^{<2>}$ and $L_i^{<3>}$ together with $L_{i+N_2}^{<1>}$, $L_{i+N_1}^{<2>}$ and $L_{i+N_1+N_2}^{<3>}$ limit a certain area. We denote the interior of this area with $\underline{E}_i$. Using $\underline{E}_i$, we can define a set E_i, which will be helpful in the next part of this paper:

$$E_i = \underline{E}_i \cup L_i^{<1>} \cup L_i^{<2>} \cup L_i^{<3>} \cup \{\mathbf{v}_i^{<1>}\} \cup \{\mathbf{q}_i\}.$$

The areas constructed in this manner are congruent, which results from Eq. 1 (of course, if one takes into account periodicity of the surface in relation to α). Moreover, none of these areas overlap each other and all of them fill the space $S^{<\alpha\zeta>}$ completely.

One can understand a two directional partitioning as a particular case of a three directional one, where the length of the segment $L_i^{<3>}$ has been reduced to null. Then $\mathbf{v}_i^{<1>} = \mathbf{q}_i$, $\mathbf{v}_i^{<2>} = \mathbf{q}_{i+N_2}$ etc., so E_i is enclosed by segments $L_i^{<1>}$, $L_i^{<2>}$ and $L_{i+N_2}^{<1>}$, $L_{i+N_1}^{<2>}$.

Reducing the length of $L_i^{<3>}$ to null causes the direction stated by parastichies from the set $P_l^{N_1+N_2}$ to become more difficult to observation, as particular areas contact with each other not along a line but only in one point. For example, areas E_i and $E_{i+N_1+N_2}$ are in contact not along $L_{i+N_1+N_2}^{<3>}$ but only in the point $\mathbf{q}_{i+N_1+N_2}$ (Fig. 4(b)).

4. Phyllotaxis on a cylindrical surface and on a conical one

Below, we describe a cylindrical surface as a space in the coordinate system $Oxyz$ and mark it by $S_{cyl}^{<xyz>}$. Similarly we mark a conical surface in the system $Oxyz$ by $S_{cone}^{<xyz>}$.

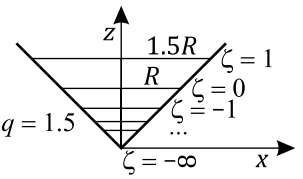

Fig. 5. Side view of a cone; there are shown cross-sections for various values of ζ.

If a point $\mathbf{q}(\alpha, \zeta) \in S^{<\alpha\zeta>}$ is given, then we can calculate the coordinates of its equivalent in the space $S_{cyl}^{<xyz>}$ using the following formulas:

$$x = R\cos\alpha, \quad y = R\sin\alpha, \quad z = Z\zeta, \tag{2}$$

where R and Z are predefined.

Analogically, we can calculate coordinates of $\mathbf{q}(\alpha, \zeta)$ in the space $S_{cone}^{<xyz>}$ using the formulas:

$$x = Rq^{\zeta}\cos\alpha, \quad y = Rq^{\zeta}\sin\alpha, \quad z = Zq^{\zeta}, \tag{3}$$

where R, Z and q are predefined.

After applying Eq. 2, the space $S^{<\alpha\zeta>}$ transforms into a cylindrical surface having the following properties:

(1) For $\zeta \in (-\infty, +\infty)$ $z \in (-\infty, +\infty)$ and if $\zeta = 0$, then $z = 0$.

(2) A cross-section of the cylinder surface is a circle of the radius R.

On the other hand, after applying Eq. 3, the space $S^{<\alpha\zeta>}$ transforms into a cone surface. Their properties are as follows:

(1) For $\zeta \in (-\infty, +\infty)$ $z \in (0, +\infty)$ and if $\zeta \to -\infty$, then $z \to 0$.

(2) If $\zeta = 0$ we obtain a cross-section being a circle of the radius R located on the plane $z = 1$.

(3) If $\zeta = 1$ we obtain a cross-section being a circle of the radius Rq located on the plane $z = q$ (Fig. 5).

Let us study two areas in the space $S^{<\alpha\zeta>}$ described in Chapter 3. We denote them by E_{i_1} and E_{i_2}. We know that $E_{i_1} \equiv E_{i_2}$ (where $\equiv$ is a symbol of congruency) and that they have an identical orientation. It means that there exists a translation described by two constants c_α, c_ζ such that if a point $\mathbf{p}^{<1>}(\alpha_1, \zeta_1) \in E_{i_1}$ exists, then there also exists the point $\mathbf{p}^{<2>}(\alpha_2, \zeta_2) \in E_{i_2}$ described by the equation:

$$\mathbf{p}^{<2>}(\alpha_2, \zeta_2) = \mathbf{p}^{<1>}(\alpha_1 + c_\alpha, \zeta_1 + c_\zeta).$$

After transforming $\mathbf{p}^{<1>}$ and $\mathbf{p}^{<2>}$ into the space $S_{cyl}^{<xyz>}$ by Eq. 2, we obtain $\mathbf{p}_{cyl}^{<1>} = (R\cos\alpha, R\sin\alpha, Z\zeta)$ and $\mathbf{p}_{cyl}^{2} = (R\cos(\alpha + c_\alpha), R\sin(\alpha + c_\alpha), Z(\zeta + c_\zeta))$. This means that $\mathbf{p}_{cyl}^{<1>} \equiv \mathbf{p}_{cyl}^{<2>}$ (are congruent), which in this case is a superposition of translation

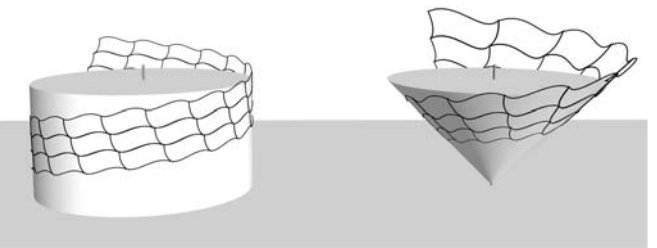

Fig. 6. Covering a cylindrical surface with congruent sets and a conical surface with similar ones; the sets of each kind completely cover their respective spaces.

along the z axis by c_ζ and rotation by an angle c_α. It is evident that the mentioned sets are also congruent in the space S^{xyz}_{cyl}, which we write down as $E_{i_1} \equiv E_{i_2}$.

After transforming these same points $\mathbf{p}^{<1>}$ and $\mathbf{p}^{<2>}$ from $S^{<\alpha\zeta>}$ into S^{xyz}_{cone} by Eq. 3, we obtain $\mathbf{p}^{<1>}_{cone} = (Rq^{\zeta_1}\cos\alpha_1, Rq^{\zeta_1}\sin\alpha_1, q^{\zeta_1})$ and $\mathbf{p}^{<2>}_{cone} = (Rq^{\zeta_1+c_\zeta}\cos(\alpha_1 + c_\alpha), Rq^{\zeta_1+c_\zeta}\sin(\alpha_1 + c_\alpha), q^{\zeta_1+c_\zeta})$. So we see that $\mathbf{p}^{<1>}_{cone} \sim \mathbf{p}^{<2>}_{cone}$, where $\sim$ stands for similarity, which in this case is a result of superposition of scaling with the scale factor q^{c_ζ} and rotation by an angle c_α. It appears that, for $S^{<xyz>}_{cone}$, $E_{i_1} \sim E_{i_2}$. Using Eq. 3 results in complete covering the cone surface $S^{<xyz>}_{cone}$ with similar areas (Fig. 6).

5. Partitioning the interior of a cylinder and a cone

Let us introduce a three-dimensional space $S^{<\alpha\zeta\rho>}$, which is understood as a generalization of $S^{<\alpha\zeta>}$. This allows us to consider $S^{<\alpha\zeta>}$ as a cross-section of $S^{<\alpha\zeta\rho>}$ for a given ρ, namely $S^{<\alpha\zeta>}(\rho)$. Similarly, as it was described in Chapter 3, we divide the space $S^{<\alpha\zeta>}(\rho)$ into sets $E_i(\rho)$ using the genetic helix (passing through the point $\mathbf{q}_0(\rho)$). As $\mathbf{q}_0(\rho)$ is dependent on ρ, it means that appropriate parastichies and segments of lines being borders of the areas $E_i(\rho)$ are dependent on ρ too. We express that by using the notation $L^{<1>}_{i+N_2}(\rho)$, $L^{<2>}_{i+N_1}(\rho)$ and $L^{<3>}_{i+N_1+N_2}(\rho)$.

The dependence of $\mathbf{q}_0(\rho)$ on ρ implies that the set $\{\mathbf{q}_0(\rho)\}$ is a segment of a certain line, which we call *a path*. For a given $\{\mathbf{q}_0(\rho)\}$, segments of lines describing borders of $E_0(\rho)$ are denoted by $L^{<1>}_{N_2}(\rho)$, $L^{<2>}_{N_1}(\rho)$ and $L^{<3>}_{N_1+N_2}(\rho)$, because $i = 0$.

Taking into account how the points $\mathbf{q}_i(\rho)$ depend on $\mathbf{q}_0(\rho)$ we notice that for each i_1, $i_2 \in \{0, \pm1, \pm2, ...\}$ and for a fixed ρ the paths $\{\mathbf{q}_{i_1}(\rho)\}$ and $\{\mathbf{q}_{i_2}(\rho)\}$ are congruent, which we show by using the notation $\{\mathbf{q}_{i_1}(\rho)\} \equiv \{\mathbf{q}_{i_2}(\rho)\}$.

Consider the set of points $V^{<\alpha\zeta\rho>} \in S^{<\alpha\zeta\rho>}$, defined as follows: $\alpha \in \langle -\pi, \pi)$, $\zeta \in (-\infty, +\infty)$, $\rho \in (r_{min}, r_{max}\rangle$ (Fig. 7(a)). Let us divide $V^{<\alpha\zeta\rho>}$ into subsets $V_i^{<\alpha\zeta\rho>}$,

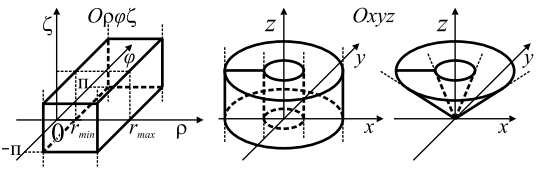

Fig. 7. From left: sets $V^{<\alpha\zeta\rho>}$, V_{cyl}^{xyz} and V_{cone}^{xyz}.

which are further referred to as subspaces. Each subspace is defined as follows:

$$V_i^{<\alpha\zeta\rho>} = \bigcup_{\rho\in(r_{min},r_{max})} E_i(\rho) \tag{4}$$

This equation shows that $E_i(\rho)$ is a cross-section of $V_i^{<\alpha\zeta\rho>}$ for a given ρ. Taking into account the congruency of $E_i(\rho)$, we see that subspaces $V_i^{<\alpha\zeta\rho>}$ are congruent too, completely fill $S^{<\alpha\zeta\rho>}$ and do not intersect each other. In fact, in order to create $V_i^{<\alpha\zeta\rho>}$, we simply sweep a variable cross-section $E_i(\rho)$ along a path $\{\mathbf{q}_i(\rho)\}$. This manner of description of three-dimensional solids is known in computer graphics as *sweep representation* [6].

Below, we consider a transformation of points $\mathbf{q}(\alpha,\zeta,\rho) \in V_i^{<\alpha\zeta\rho>}$ into the space $S_{cyl}^{<xyz>}$ or $S_{cone}^{<xyz>}$, respectively, in accordance with the following equations:
for a cylinder

$$x = \rho\cos\alpha, \quad y = \rho\sin\alpha, \quad z = Z\zeta \tag{5}$$

and for a cone

$$x = \rho q^{\zeta}\cos\alpha, \quad y = \rho q^{\zeta}\sin\alpha, \quad z = Zq^{\zeta} \tag{6}$$

In the space $S_{cyl}^{<xyz>}$, the set $V^{<\alpha\zeta\rho>}$ obtains a shape of a drilled cylinder, which is marked by the symbol $V_{cyl}^{<xyz>}$ (Fig. 7(b)), while in the space $S_{cone}^{<xyz>}$, it obtains a shape of drilled cone which is marked by $V_{cone}^{<xyz>}$ (Fig. 7(c)). Subspaces being results of transformations $V_i^{<\alpha\zeta\rho>}$ are marked by $V_{cyl,i}^{<xyz>}$ and $V_{cone,i}^{<xyz>}$.

Figure 8 represents a space $V_i^{<\alpha\zeta\rho>}$ in the case when $L_i^{<1>}(\rho)$, $L_i^{<2>}(\rho)$ and the path $\{\mathbf{q}_0(\rho)\}$ are segments of straight lines. Moreover, two corresponding subspaces: $V_{cyl,i}^{<xyz>}$ and $V_{cone,i}^{<xyz>}$ are shown. Figure 9 explains how the subspaces $V_{cyl,i}^{<xyz>}$ and $V_{cone,i}^{<xyz>}$ can fill a cylindrical space and a conical one for both two- and three-directional partitioning.

Below, there are more complicated examples of two-directional partitioning. One can easily imagine analogous examples for a three-directional case comparing these examples with Fig. 6. Figure 10(a) illustrates a subspace $V_i^{<\alpha\zeta\rho>}$, which has its path being a segment of straight line, while $L_i^{<1>}(\rho)$, $L_i^{<2>}(\rho)$ are segments of curves changing

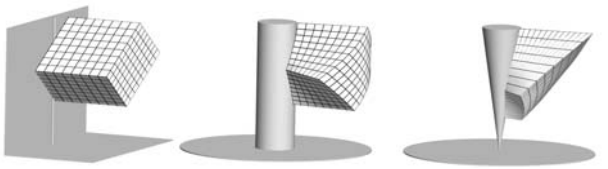

Fig. 8. From left: an example of a subspace $V_i^{<\alpha\zeta\rho>}$ and two corresponding subspaces $V_{cyl,i}^{<xyz>}$ and $V_{cone,i}^{<xyz>}$.

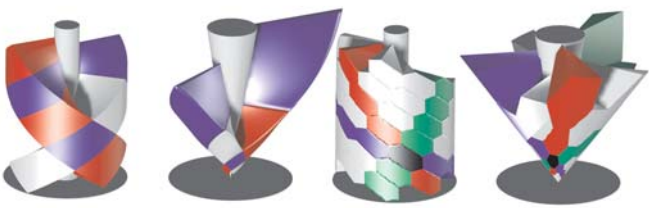

Fig. 9. Examples of a cylinder space and a cone one filled by subspaces $V_{cyl,i}^{<xyz>}$ and $V_{cone,i}^{<xyz>}$ for both the two- and the three-directional partitioning.

their shapes depending on ρ. Fig. 10(b) shows a subspace $V_{cyl,i}^{<xyz>}$ being a result of transformation for the input subspace from Fig. 10(a). Figure 10(c) shows a cylinder subspace constructed by these same lines $L_i^{<1>(\rho)}$, $L_i^{<2>(\rho)}$ and the path being a curve lying on a plane $\alpha = const.$ In Fig. 10(d) there is a similar example but the path is a curve lying on a plane $\zeta = const.$

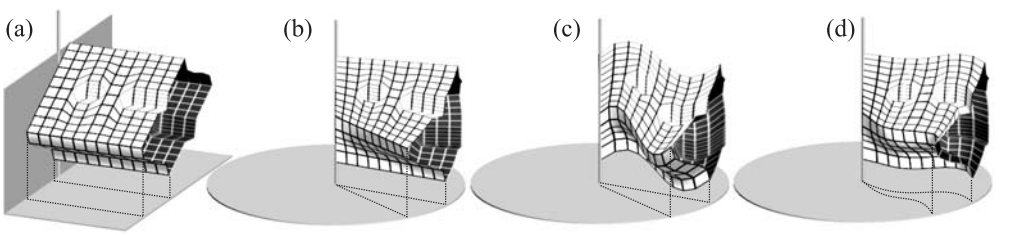

Fig. 10. Examples: (a) a subspace $V_i^{<\alpha\zeta\rho>}$ and various subspaces $V_{cyl,i}^{<xyz>}$ (b, c, d); the front faces have been removed in order to reveal the interiors.

Fig. 11. Filling the cylinder interior by subspaces $V_{cyl,i}^{<xyz>}$; left: three models where modules originate respectively from Fig. 10(b), (c) and (d), right: a three-directional model.

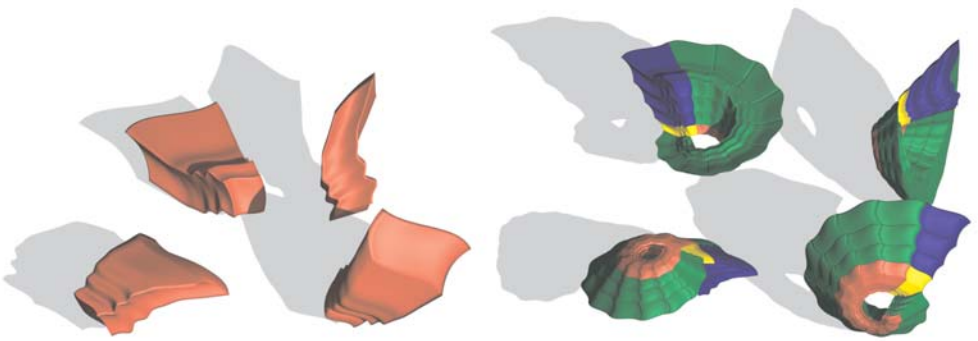

Fig. 12. An example of a subspace $V_{cone,i}^{<xyz>}$ (left) and the result of filling a cone interior (right).

Figure 11 (left) shows a manner of filling the cylinder space by subspaces $V_{cyl,i}^{<xyz>}$ from Fig. 10(b), (c) and (d). Subspaces lying on a certain chosen parastichy $P_j^{N_1}$ and on a certain $P_k^{N_2}$ have been distinguished respectively by colors: red and blue, whereas a subspace located on the intersection of both these parastichies—by yellow. On the right side of this figure a model with three-directional filling is shown.

Figure 12 shows an example of a certain subspace $V_{cone,i}^{<xyz>}$ and a result of filling a cone interior with subspaces similar to $V_{cone,i}^{<xyz>}$.

6. Arranging non-intersecting modules inside a cylinder or a cone

When natural objects having their modules arranged in accordance with the phyllotaxis rules are modeled, it is often essential for them not to intersect each other. In order to meet this requirement we can use the idea of subspaces $V_i^{<\alpha\zeta\rho>}$, $V_{cyl,i}^{<xyz>}$ and $V_{cone,i}^{<xyz>}$, $(i = 0, \pm1, \pm2,...)$ discussed in Chapter 5.

Let us associate a certain set $M_i^{<\alpha\zeta\rho>}$, called *module*, with each subspace $V_i^{<\alpha\zeta\rho>}$. Assume that the following relation is true:

$$M_i^{<\alpha\zeta\rho>} \subseteq V_i^{<\alpha\zeta\rho>} \tag{7}$$

This relation remains true also after transforming a module $M_i^{<\alpha\zeta\rho>}$ into the cylindrical space or into the conical one. Thus for a cylinder

$$M_{cyl,i}^{<xyz>} \subseteq V_{cyl,i}^{<xyz>} \tag{8}$$

and for a cone

$$M_{cone,i}^{<xyz>} \subseteq V_{cone,i}^{<xyz>} \tag{9}$$

In the case of a cylinder, if we assume that all the modules are congruent, then we can work out the shape of a module in the space $S^{<\alpha\zeta\rho>}$. Next, after doing the test described by Eq. 7, we should copy this module and put the duplicates in the appropriate places of this space. In the end, the whole group of modules is transformed into the cylinder space.

Alternatively we can work out the shape of a module in the space $S_{cyl}^{<xyz>}$, execute the test in accordance with Eq. 8 and, in the end, copy the module to put its duplicates in places being occupied by the subspaces $V_{cyl,i}^{<xyz>}$. We should remember that it is not necessary to restrict our activity to the case when modules are congruent to each other, in contrast to the case of subspaces. It is only essential for each module to satisfy Eq. 8. This ensures that the area of applications of the described method is wider.

In the case of cones, variants of the procedure are analogous but requirements relating to congruency of the modules in the space $S_{cyl}^{<xyz>}$ should be replaced with requirements relating to the similarity in $S_{cone}^{<xyz>}$. In addition, the test described by Eq. 9 should be applied instead of the test in Eq. 8.

Figure 13 shows objects resembling leaves arranged inside a cylinder. The corresponding subspaces are shown too. Figure 14(a) represents a cylindrical model, consisting of 160 modules with shapes that vary depending on their positions along the z axis. Here, the subspaces from Fig. 13(d) have been used. Fig. 14(b) represents a conical model consisting of the same modules. Figure 15 shows a model of inflorescence consisting of two parts: the upper one—conical and the lower one—cylindrical. Each part contains

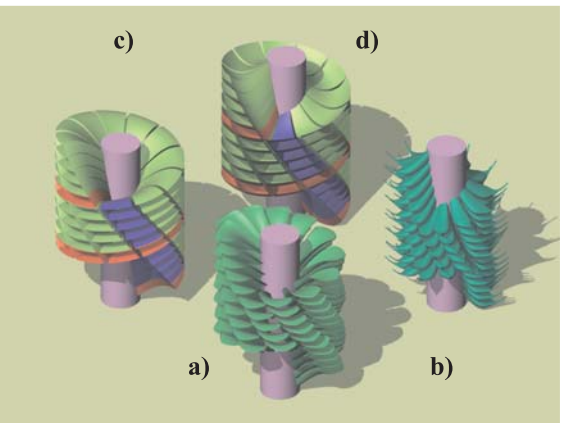

Fig. 13. Two models, (a) and (b), consisting of non-intersecting modules, each resembling a leaf on a stem, and two sets of subspaces corresponding with these models, shown in (c) and (d), respectively.

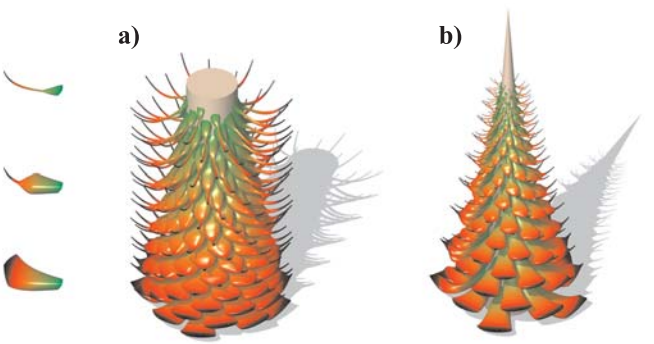

Fig. 14. A cylindrical model (a) consisted of modules having their shapes dependent on the module position along the model axis, and a conical one (b) consisted of the same modules.

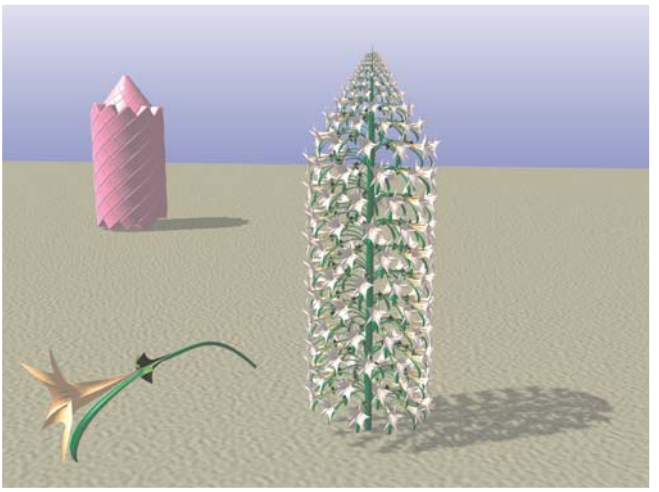

Fig. 15. On the right, an inflorescence consisting of two parts: the conical upper part and the cylindrical lower one; on the left, a module is shown in the foreground while in the background we can see partitioning a cone and a cylinder into subspaces appropriate for this model.

120 non-intersecting modules arranged in concordance with the rules described herein. Each module consists of a flower, a leaf and a stalk.

To sum up, in order to construct a model, namely the set $\{M_{cyl,i}^{<xyz>}\}$ or $\{M_{cone,i}^{<xyz>}\}$ one should perform the following steps:

Begin

1) Determine the phyllotaxis parameters, namely the parameters of the genetic helix and parameters of parastichies in dependence on a chosen partitioning: two- or three-directional;
2) Determine a path $\mathbf{q}_0(\rho)$ in the space $S^{<\alpha\zeta\rho>}$;
3) Determine lines $L_0^{<1>}(\rho)$, $L_0^{<2>}(\rho)$, and for the three-directional partitioning also $L_0^{<3>}(\rho)$;
4) Construct an area $E_0(\rho)$ and next, basing on this area and on the path, construct a subspace $V_0^{<\alpha\zeta\rho>}$ using the sweep representation method; choose Variant A, B or C;

Variant A:

5(a) Construct the module $M_0^{<\alpha\zeta\rho>}$ in the manner which satisfies relation $M_0^{<\alpha\zeta\rho>} \subseteq V_0^{<\alpha\zeta\rho>}$;

6(a) Copy $M_0^{<\alpha\zeta\rho>}$ and arrange duplicates along the axes α and ζ in accordance with the phyllotaxis parameters, which ensure that each subspace $V_i^{<\alpha\zeta\rho>}$ containing its own module $M_i^{<\alpha\zeta\rho>}$ precisely adjoin its neighboring subspaces;

7(a) Using Eq. 5 or Eq. 6, transform the obtained set of the modules $\{M_i^{<\alpha\zeta\rho>}\}$ into the cylinder space $S_{cyl}^{<xyz>}$ or into the cone one $S_{cone}^{<xyz>}$; Go to L1; (End of Variant A);

Variant B—for a cylinder:

5(b) Using Eq. 5, transform $V_0^{<\alpha\zeta\rho>}$ into the cylinder space $S_{cyl}^{<xyz>}$ to obtain $V_{cyl,0}^{<xyz>}$;

6(b) Construct the module $M_{cyl,0}^{<xyz>}$ in the manner which satisfies the relation $M_{cyl,0}^{<xyz>} \subseteq V_{cyl,0}^{<xyz>}$;

7(b) Copy $M_{cyl,0}^{<xyz>}$, next rotate and move in accordance with the phyllotaxis parameters, in order to obtain the set $\{M_{cyl,i}^{<xyz>}\}$; Go to L1; (End of Variant B);

Variant C—for a cone:

5(c) Using Eq. 6, transform $V_0^{<\alpha\zeta\rho>}$ into the cone space $S_{cone}^{<xyz>}$ to obtain $V_{cone,0}^{<xyz>}$;

6(c) Construct the module $M_{cone,0}^{<xyz>}$ in the manner which satisfies the relation $M_{cone,0}^{<xyz>} \subseteq V_{cone,0}^{<xyz>}$;

7(c) Copy $M_{cone,0}^{<xyz>}$, next rotate, scale and move in accordance with the phyllotaxis parameters, in order to obtain the set $\{M_{cone,i}^{<xyz>}\}$; (End of Variant C);

L1: **End**

7. Conclusion

The method described in this paper makes it possible to construct modules and arrange them in accordance with phyllotaxis rules in such a way that they do not intersect each other. One can create the modules using the conception of a subspace in the space $V^{<\alpha\zeta\rho>}$ or alternatively in the respective spaces $V_{cyl}^{<xyz>}$ or $V_{cone}^{<xyz>}$. A diversity of shapes is a result of creation subspaces using the so called *sweep representation* method by moving a cross-section along a given path. The curvilinear paths are allowed as well as such cross-sections that change their shapes along the path. The appropriate requirements related to the cross-section shape in the space $V^{<\alpha\zeta\rho>}$ ensure the congruency of subspaces inside a cylinder as well as similarity inside a cone and at the same time the absence of mutual intersections of subspaces. The advantage of the described method consists in the following: if there is given a certain partitioning into subspaces then one

can place inside these subspaces modules differing from each other in shapes, as it can be observed in nature. The method enables us to construct complicated models composed of certain parts being cylinders and at the same time of other parts being cones (Fig. 15). This approach can be useful in practical applications. The author hopes that the method described herein can be applicable to modeling not only modular plants but also other objects of a cylindrical or conical shape, consisting of regularly arranged modules.

References

1990
[1] Prusinkiewicz P., Lindenmayer A.: The Algorithmic Beauty of Plants. Springer Verlag.
1992
[2] Douady S., Couder Y.: Phyllotaxis as a Physical Self-Organized Growth Process. Physical Review Letters. Vol. 68.
[3] Fowler D.R., Prusinkiewicz P., Battjes J.: A collision-based model of spiral phyllotaxis. Proc. of the 19th Annual Conference on Computer Graphics and Interactive Techniques SIGGRAPH'92.
1994
[4] Zagórska-Marek B.: Phyllotaxic diversity in Magnolia flowers, Acta Soc. Bot. Poloniae 63 117-137.
1996
[5] Douady S., Couder Y.: Phyllotaxis as a Dynamical Self Organizing Process. Journal of Theoretical Biology. 178, 255-274.
[6] Foley I. et al.: Computer Graphics: Principles and Practice. Addison-Wesley.
1997
[7] Adler I., Barabe D., Jean R.V.: A History of the Study of Phyllotaxis. Annals of Botany 80: 231-244.
1998
[8] Cummings F.W., Strickland J.C.: A Model of Phyllotaxis. Journal of Theoretical Biology 192, 531-544.
2000
[9] Hargittai I., Pickover C.A.: Spiral symmetry. World Scientific Publishing.
2004
[10] Kappraff J.: Growth in Plants: A Study in Number. Forma, 19, 335-354.
2005
[11] Shipman P.D., Newell A.C.: Polygonal planforms and phyllotaxis on plants. Journal of Theoretical Biology, 236, 154-197.
2006
[12] Smith R.S., Kuhlemeier C., Prusinkiewicz P.: Inhibition fields for phyllotactic pattern formation: a simulation study. Canadian Journal of Botany 84(11), pp. 1635-1649.
[13] Ciszak Ł., Stępień C.: A dynamic model of phyllotaxis for application in computer graphics. Proceedings of the XII National Conference Application of Mathematics to Biology and Medicine, Koninki, Poland, pp. 31-36.
2008
[14] Newell A.C., Shipman P.D., Sun Z.: Phyllotaxis: Cooperation and competition between mechanical and biochemical processes. Journal of Theoretical Biology, 251, 421-439.
[15] Zagórska-Marek B., Szpak M.: Virtual phyllotaxis and real plant model cases. Functional Plant Biology, 35, 1025-1033.
2009
[16] Nisoli C., Gabor N.M., Lammert P.E., Maynard J.D., Crespi V.H.: Static and Dynamical Phyllotaxis in Magnetic Cactus. Physical Review Letters. 102.
2014
[17] http://www.fosterandpartners.com/Projects/1004/Default.aspx, Swiss Re H, 30 St Mary Axe (retrieved Feb. 1, 2014).